IOPscience iopscience.iop.org

Home Search Collections Journals About Contact us My IOPscience

Optical and electron paramagnetic resonance spectroscopy of $Cd_{1-x}Mn_xS$ quantum dots

This article has been downloaded from IOPscience. Please scroll down to see the full text article.

2004 J. Phys.: Condens. Matter 16 4625

(http://iopscience.iop.org/0953-8984/16/25/020)

View the table of contents for this issue, or go to the journal homepage for more

Download details:
IP Address: 129.252.86.83
The article was downloaded on 27/05/2010 at 15:38

Please note that terms and conditions apply.

INSTITUTE OF PHYSICS PUBLISHING JOURNAL OF PHYSICS: CONDENSED MATTER

J. Phys.: Condens. Matter **16** (2004) 4625–4633 PII: S0953-8984(04)75205-4

Optical and electron paramagnetic resonance spectroscopy of $Cd_{1-x}Mn_xS$ quantum dots

B Babić Stojić, D Milivojević, M Čomor and V Vodnik

Vinča Institute of Nuclear Sciences, PO Box 522, 11001 Belgrade, Serbia and Montenegro

Received 21 January 2004
Published 11 June 2004
Online at stacks.iop.org/JPhysCM/16/4625
doi:10.1088/0953-8984/16/25/020

Abstract

$Cd_{1-x}Mn_xS$ quantum dots (QDs) with diameter $d \leqslant 4.5$ nm and with manganese concentrations from $x = 0.001$ to 0.15 have been prepared using aqueous solution precipitation. Absorption and fluorescence spectra at room temperature have been recorded. No monotonic variation of the band gap energy with increasing manganese concentration is observed. The electron paramagnetic resonance (EPR) measurements were performed on a 9.5 GHz spectrometer in the temperature range 20–290 K. Two structures in the EPR spectra are observed for all the manganese concentrations: a hyperfine structure and a broad EPR line. The hyperfine structure is described by allowed and forbidden hyperfine transitions of the Mn^{2+} ion central sextet with hyperfine splitting constant $|A| = 9.6$ mT and with axial-field splitting parameter D ranging from 11.1 to 13.5 mT. The hyperfine structure is attributed to the isolated Mn^{2+} ions at or near the surface of the nanocrystals. The width of the broad resonance and its temperature independence suggest that the wide line originates from the noncentral manganese transitions broadened by crystal-field effects, as in some disordered materials.

1. Introduction

Semiconductor nanocrystals have changed physical properties compared with the bulk crystalline materials and show significant departure from the bulk optical and electronic properties when the particle size becomes comparable to or smaller than the exciton Bohr radius (a_B). In this limit the energy level scheme will depend on the size and shape of crystallite. The energy of the lowest excited state shifts to higher energy as the particle size decreases [1]. This property is observed in many metal-chalcogenides (CdS, PbS, ZnS, HgSe, ZnSe, ...), metal-chalogenides ($AgBr, PbI_2, \ldots$) and oxides (TiO_2, ZnO)—so-called nanocrystal quantum dots (QDs)—and is understood as a quantum size effect resulting from the confinement of an electron and hole in a small volume [2–5]. In manganese-doped ZnS nanocrystals, apart from the increasing band gap energy E_g with decreasing size, the spatial confinement of

 © 2004 IOP Publishing Ltd Printed in the UK

the electron and hole and the corresponding increase in their overlap with the localized d-electron states provide fast energy transfer of electron–hole pairs to the Mn^{2+} ion impurity and subsequent large photoluminescent efficiency and much faster radiative recombination of d-electron excitation than in the bulk crystals [6]. Very high photoluminescent efficiency was also obtained from Mn-doped ZnSe nanocrystals with the Mn^{2+} ions embedded inside the nanoparticles [7]. The photoluminescence and EPR hyperfine structure due to isolated Mn^{2+} ions in a tetrahedral coordination were observed in $Cd_{1-x}Mn_xS$ nanocrystals for manganese concentrations larger than in the bulk [8, 9]. In these works the synthesis of $Cd_{1-x}Mn_xS$ QDs was based on the usage of reverse micelles as templates in order to control their size (from 1.8 to 4 nm) and composition (from $x = 0.03$ to 0.3). In a recent study of manganese-doped CdSe nanocrystals prepared with a high-temperature reaction it was found that most of the dopant atoms segregated to the particle surface [10].

The quality of nanocrystals and distribution of dopant atoms, which depend on the method of preparation, strongly influence their optical and magnetic properties. In this paper we present optical and EPR studies of $Cd_{1-x}Mn_xS$ QDs with diameter $d \leqslant 4.5$ nm prepared using different synthetic procedure compared to those already described in the literature.

2. Experimental details

2.1. Preparation of $Cd_{1-x}Mn_xS$ QDs

Colloidal dispersions consisting of $Cd_{1-x}Mn_xS$ QDs with $d \leqslant 4.5$ nm were prepared by mixing a solution containing $Cd(NO_3)_2$ and $MnSO_4$ with a solution containing Na_2S in the presence of surface active agent sodium hexametaphosphate $(NaPO_3)_6$. The concentration of cations ($[Cd^{2+}] + [Mn^{2+}]$) was constant and equal to 2×10^{-3} M, while an 'excess' of S^{2-} ions was used in the synthesis (2.4×10^{-3} M). The content of Mn^{2+} ions varied up to $x = 0.15$. The concentration of $[(NaPO_3)_6]$ was 2×10^{-2} M. Light and air were excluded during the preparation of this colloid. After precipitation of colloidal particles the solvent was removed by vacuum evaporation at room temperature. The obtained yellow powder could be redissolved in water to give a colloid with the same structured absorption spectrum as the dispersion before evaporation. The contents of cations in powders consisting of $Cd_{1-x}Mn_xS$ QDs with $d \leqslant 4.5$ nm were checked by measuring atomic absorption (ICP-AS Perkin-Elmer 6500) for Cd and Mn.

2.2. Apparatus

The x-ray diffraction analysis (Philips PW 1710 diffractometer) of $Cd_{1-x}Mn_xS$ QDs with $d \leqslant 4.5$ nm performed for various compositions showed hexagonal wurtzite crystal structure, as in the bulk phase of this material. This is consistent with the crystal structure study of CdS nanoparticles [11], where it was found that a size-induced transformation from hexagonal to cubic structure occurred for the particle diameter 4–5 nm with the equilibrium cubic zincblende phase in smaller size particles. No diffractograms corresponding to MnS or MnO were observed in our x-ray diffraction experiment.

UV–visible absorption spectra were recorded on a Perkin-Elmer Lambda 5 instrument, while fluorescence measurements were carried out using a Perkin-Elmer LS-3b instrument.

The EPR measurements were performed on a Varian spectrometer with a 9 inch magnet operating at the nominal frequency $\nu = 9.5$ GHz. The first derivative of the absorption lines was recorded. The samples were cooled in an open-cycle cryogenic refrigerator using flowing hydrogen gas.

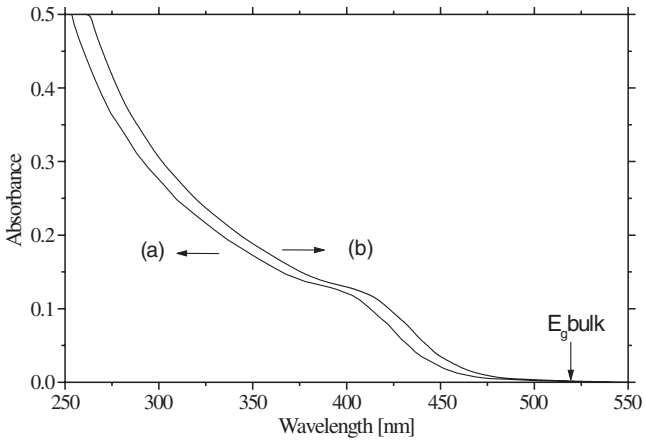

Figure 1. Absorption spectra of (a) CdS QDs and (b) $Cd_{0.9}Mn_{0.1}S$ QDs at room temperature.

Table 1. Band gap energy in several $Cd_{1-x}Mn_xS$ QDs determined from absorption spectra at room temperature.

x	0	0.001	0.01	0.10
Band gap (eV)	2.73	2.57	2.56	2.66

3. Results and discussion

An absorption spectrum of the colloid containing CdS QDs is shown in figure 1, curve (a). A blue shift of the absorption onset of about 0.3 eV compared to the bulk CdS material [12] can be noticed. This result is a direct consequence of the quantum confinement effect associated with the small particle size. The radius R of CdS QDs can be calculated using an effective mass approximation model [1]:

$$\Delta E = \left(\frac{\hbar^2\pi^2}{2R^2}\right)\left(\frac{1}{m_e} + \frac{1}{m_h}\right) - \frac{1.8e^2}{\varepsilon R}, \tag{1}$$

where $\Delta E = 0.3$ eV is the increase of the band gap energy with respect to the bulk band gap, $m_e = 0.19\, m_0$ and $m_h = 0.8\, m_0$ are the effective masses of electrons and holes in the units of free electron mass, and $\varepsilon = 5.7$ is the high frequency dielectric coefficient [1]. The calculated value for the radius of CdS QDs was found to be 2.25 nm ($d = 4.5$ nm).

An absorption spectrum of the colloid containing $Cd_{0.9}Mn_{0.1}S$ QDs is also shown in figure 1, curve (b). The absorption onset of $Cd_{0.9}Mn_{0.1}S$ QDs is slightly shifted towards longer wavelengths compared to the CdS QDs. The values of the band gap energy for several manganese concentrations in $Cd_{1-x}Mn_xS$ QDs obtained from the absorption spectra at room temperature are presented in table 1. For a given particle size no monotonic variation of the band gap energy with composition is observed. Similar behaviour of the band gap energy with composition was detected in the bulk phase of $Cd_{1-x}Mn_xS$ [12]. In the bulk phase of Mn-based diluted magnetic semiconductors the appearance of the minimum in the band gap energy with increasing manganese concentration is explained by exchange interactions of the conduction and valence band electrons with the Mn^{2+} d electrons [13]. If the same theory could be applied to nanocrystal form of the material, an increase of the exchange interactions between the Mn^{2+} d electrons and band electrons at a given temperature would

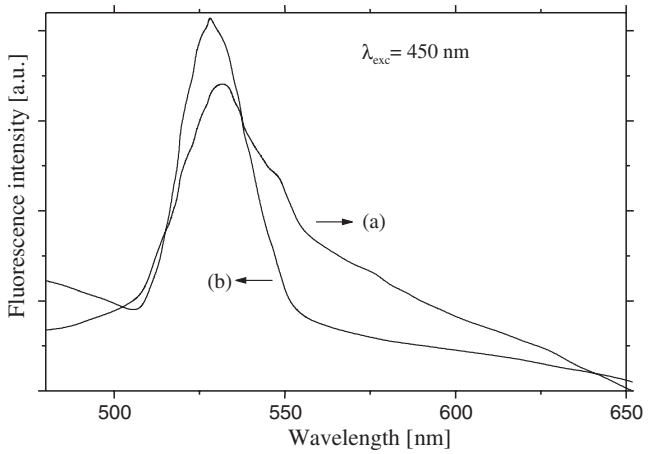

Figure 2. Fluorescence spectra of (a) CdS QDs and (b) $Cd_{0.9}Mn_{0.1}S$ QDs at room temperature ($\lambda_{exc} = 450$ nm).

lead to a deeper minimum in the $E_g(x)$ dependence. A pronounced minimum in the band gap energy versus composition was detected for very small $Cd_{1-x}Mn_xS$ nanocrystals of average particle diameter 1.8 nm [9], suggesting a significant increase of the Mn^{2+} ion-band electrons' exchange interactions compared to the bulk. The observed variation of the band gap energy with increasing manganese concentration in our $Cd_{1-x}Mn_xS$ QDs with $d \leqslant 4.5$ nm gives an indication that such interactions are present.

Room temperature fluorescence spectra of CdS and $Cd_{0.9}Mn_{0.1}S$ QDs ($\lambda_{exc} = 450$ nm) are shown in figure 2, curves (a) and (b), respectively. The fluorescence spectrum of CdS QDs is characterized by one emission band centred at about 530 nm originating from a band to band recombination, and a long wavelength emission originating from a surface defects recombination [9, 14, 15]. The position and intensity of the long wavelength emission of CdS nanoparticles depend on the mode of synthesis, particularly on the ratio of cadmium and sulfide ion concentrations [14, 15]. Although the surface active agent sodium hexametaphosphate was present in high concentration in our samples, the defect sites on the surface of CdS QDs were not completely blocked, and long wavelength emission appeared. It should be pointed out that the presence of Mn^{2+} ions induced disappearance of the long wavelength emission and an increase in the band to band emission (compare curves (a) and (b) in figure 2). The fluorescence spectrum of $Cd_{0.9}Mn_{0.1}S$ QDs suggests that the Mn^{2+} ions are probably located at or near the surface of the nanocrystals. Incorporation of the Mn^{2+} ions produces passivation of defect centres on the surface of the nanocrystals. In addition, there is no Mn^{2+}-based emission from the $^4T_1$–$^6A_1$ transition at about 580 nm which is characteristic for isolated Mn^{2+} ions in tetrahedral coordination inside the $Cd_{1-x}Mn_xS$ nanocrystals [8, 9]. A difference in the photoluminescent spectra for Mn-doped ZnS and Mn-activated ZnS nanoclusters of about 5 nm in diameter was also detected [5]. In Mn-doped ZnS nanoclusters (Mn^{2+} ions introduced inside the ZnS particles) orange emission at 585 nm was present as in the bulk ZnS doped with Mn^{2+}, whereas in Mn-activated ZnS nanoclusters (ZnS particles with surface bound Mn^{2+} ions) no Mn^{2+}-based emission from $^4T_1$–$^6A_1$ transition was observed.

The EPR spectra of $Cd_{1-x}Mn_xS$ QDs for various compositions up to $x = 0.15$ recorded at room temperature are shown in figure 3. The EPR spectra measured at lower temperatures, down to $T = 20$ K, do not differ in shape from the spectra at room temperature. Each

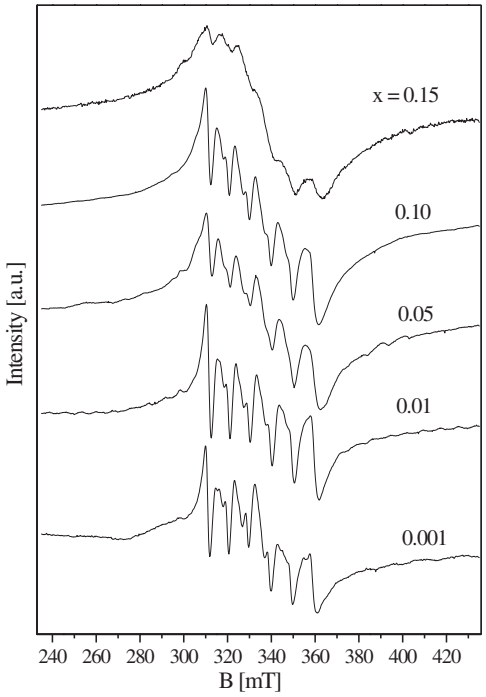

Figure 3. EPR spectra of $Cd_{1-x}Mn_xS$ QDs at room temperature.

spectrum consists of a group of narrow lines superimposed on a broad resonance. The narrow lines are composed of six allowed hyperfine lines and pairs of forbidden hyperfine transitions between the allowed hyperfine lines. The intense forbidden transitions are characteristic for some polycrystalline and disordered materials [16], reflecting a distortion of the crystal lattice around the Mn^{2+} ions from cubic symmetry which varies from ion to ion. We take the following spin Hamiltonian to describe the EPR spectra of an Mn^{2+} ion in $Cd_{1-x}Mn_xS$ nanocrystals:

$$H = g\mu_B \mathbf{B}\cdot\mathbf{S} + D[S_z^2 - \tfrac{1}{3}S(S+1)] + A\mathbf{S}\cdot\mathbf{I} \tag{2}$$

where $S = 5/2$ is the electron spin and $I = 5/2$ is the nuclear spin of the Mn^{2+} ion, $\mathbf{B}$ is the applied magnetic field, A is the hyperfine splitting constant, D is the axial-field splitting parameter, and g and μ_B are the Landé factor and Bohr magneton respectively.

The structure of the Mn^{2+} ion hyperfine spectrum in our samples corresponds to the typical central hyperfine sextet: the allowed hyperfine lines include transitions ($M = 1/2$, $m \leftrightarrow M = -1/2$, m) ($\Delta M = \pm 1$, $\Delta m = 0$), where $m = -5/2, -3/2, -1/2, +1/2, +3/2, +5/2$, and five hyperfine forbidden doublets due to transitions ($M = 1/2$, $m \leftrightarrow M = -1/2$, $m - 1$), and ($M = 1/2, m - 1 \leftrightarrow M = -1/2, m$) ($\Delta M = \pm 1, \Delta m = \pm 1$), where $m = -3/2, -1/2, +1/2, +3/2, +5/2$. The eigenvalues of the Hamiltonian (2) were calculated up to the third order in perturbation [16]. On the basis of these eigenvalues we have derived the positions of the allowed and forbidden hyperfine transitions of the Mn^{2+} ion central sextet. The intensities of the hyperfine lines have been calculated by taking a random orientation of the axial symmetry axis relative to the external magnetic field and assuming equal intensities of all allowed transitions and equal intensities of all forbidden transitions. In addition to the hyperfine lines, a resonance of Lorentzian type is also included in the theoretical spectra. The theoretical spectral functions were fitted to the experimental traces of the absorption lines. The

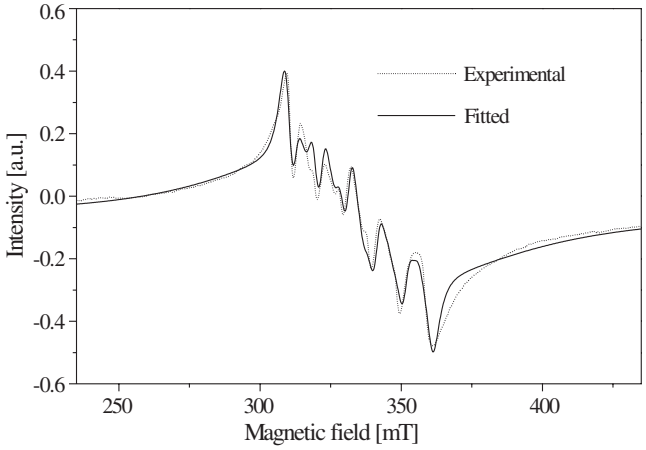

Figure 4. Experimental and fitted EPR spectrum of $Cd_{1-x}Mn_xS$ QDs with $x = 0.10$.

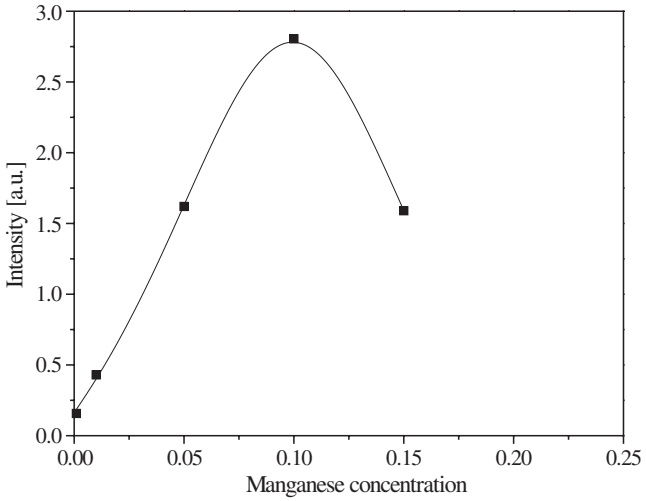

Figure 5. Intensity of the allowed hyperfine transition lines at room temperature as a function of manganese concentration. The curve is just a guide to the eye.

results are presented in table 2, and in figures 4–6. Figure 4 shows the experimental and fitted EPR spectrum of $Cd_{1-x}Mn_xS$ QDs with $x = 0.10$.

It is well known that the hyperfine interaction between the electron and nuclear spin of the Mn^{2+} ion is strongly dependent on the local environment, and that the EPR spectra can be used to determine the location of the Mn. The hyperfine splitting constant obtained for our $Cd_{1-x}Mn_xS$ QDs is $|A| = 9.6 \pm 0.2$ mT. This value agrees well with that established for Mn^{2+} ions located near the surface of CdS:Mn nanocrystals, 9.6 mT [18], near the surface of ZnS:Mn nanocrystals, 9.5 mT [19], and in the surface layers of Mn-doped CdSe nanocrystals, 8.9 mT [10]. The hyperfine splitting constant of the Mn^{2+} ions substitutionally incorporated in the nanoparticles has systematically lower values. Inside the CdS:Mn nanocrystals the parameter A is 6.9 mT [18], in the ZnS:Mn nanoparticles also 6.9 mT [17], and in the Mn-doped ZnSe nanocrystals 6.5 mT [7]. The variation of the hyperfine splitting constant is

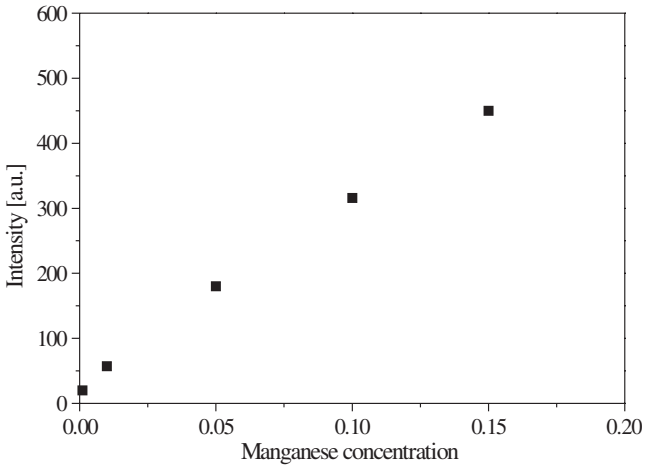

Figure 6. Intensity of the broad resonance at room temperature as a function of manganese concentration.

Table 2. Hyperfine splitting constant $|A|$, axial-field splitting parameter D and broad resonance linewidth ΔB_L as a function of manganese concentration for $Cd_{1-x}Mn_xS$ QDs.

x	$\|A\|$ (mT)	D (mT)	ΔB_L (mT)
0.001	9.5	11.1	43
0.01	9.5	11.4	—
0.05	9.6	11.4	46
0.10	9.6	11.3	45
0.15	9.8	13.5	33

explained by the change of covalence of the chemical bonds. The more ionic bonding of the ion in the lattice leads to the larger hyperfine splitting. One could expect a decrease of the covalence of the Mn–S bonds in going from the core to the surface of the nanocrystal. The hyperfine splitting constant for isolated Mn^{2+} ions obtained in this work differs from that in the bulk CdS, $A_{bulk} = -7$ mT [20], and is much closer to the parameter A for Mn^{2+} in $KMgF_3$, 9.8 mT [19], and for Mn^{2+} in borate glasses, 9.3 mT [16], which are more ionic than CdS.

Our EPR spectra also reveal that the Mn^{2+} ion sites are exposed to the crystal field of axial (or lower) symmetry. The axial-field splitting parameter D obtained by fitting the theoretical spectral functions to the experimental spectra is found to vary from 11.1 mT for $x = 0.001$ to 13.5 mT for $x = 0.15$. Although the parameter D is determined from the second and third order in perturbation so that the error in its determination is of the order of the observed variation, this parameter is much larger than that for Mn^{2+} in the bulk hexagonal CdS, $D_{bulk} = 0.9$ mT [20], and close to the average value of the fine structure parameter seen in borate glasses, 9.5 mT [16]. The enhanced hyperfine splitting and crystal-field strength on the axially perturbed Mn sites, which we have detected for isolated Mn^{2+} ions in $Cd_{1-x}Mn_xS$ QDs, suggest that the Mn^{2+} ions are located at or near the surface of the nanocrystals.

The intensity of the allowed transition lines determined as integral of the first derivative of the absorption lines, and obtained by fitting the theoretical spectral lines to the experimental traces at room temperature, is presented as a function of manganese concentration in figure 5. This intensity has its maximum around $x = 0.10$. This dependence is in accordance with the assumption that most of the Mn^{2+} ions are at the surface of the nanocrystals. In a nanoparticle

of $Cd_{1-x}Mn_xS$ with diameter of 4.5 nm there are about 1000 molecules. About 1/3 of this number is on the surface of the nanocrystal. The number of Mn^{2+} ions per one nanoparticle increases with increasing manganese concentration. We estimate that even in the sample with $x = 0.10$ the average number of Mn^{2+} ions per nanoparticle can be arranged on the surface as isolated ions and contribute to the EPR hyperfine structure. The authors in [8] also observed a maximum in the photoluminescence intensity of $Cd_{1-x}Mn_xS$ nanoparticles for $x = 0.08$ and a maximum in the intensity of the EPR hyperfine lines around $x = 0.05$. We think that the maximum number of isolated Mn^{2+} ions observed in our experiment around $x = 0.10$ is a consequence of the distribution of the Mn^{2+} ions at the surface of the nanocrystals. This assumption is supported by the fact that there is no band centred at 580 nm in our fluorescence spectra which could appear if the isolated ions were in the regular tetrahedral sites inside the CdS matrix. For larger manganese concentration, $x = 0.15$, most of the Mn^{2+} ions at the surface of the particles with $d \leqslant 4.5$ nm should be the nearest-neighbours, and only a small part can remain isolated, leading to a decrease of the hyperfine line intensity (figure 5).

The broad resonance is centred around $g = 2$. The linewidth of the broad resonance ΔB_L, determined as the half width at half maximum of the Lorentzian curve and obtained as a fitting parameter, is also presented in table 2. No temperature dependence of the linewidth ΔB_L was observed, nor any significant dependence on the manganese concentration. Such characteristics of the broad resonance suggest that it is an inhomogeneously broadened line originating from the noncentral manganese transitions. Figure 6 shows the intensity of the broad resonance as a function of manganese concentration. This intensity was also determined as the integral of the first derivative of the absorption lines, and obtained by fitting the theoretical spectral lines to the experimental traces at room temperature. It is seen that this intensity, which can be used as a measure of the total number of Mn^{2+} ions in the samples, increases with increasing manganese concentration. A decrease or disappearance of the wide line intensity was not observed down to $T = 20$ K, showing that there is no MnS phase in our samples in which strong antiferromagnetic interaction between the Mn^{2+} ions is expected. The wide line is composed of the individual manganese noncentral transitions broadened by the crystal field in their surroundings. The exchange interaction between the nearest-neighbour Mn^{2+} ions seems to be relatively weak. This interaction has no significant influence on the broad resonance linewidth such as that observed in some $Cd_{1-x}Mn_xS$ QDs with the Mn^{2+} ions inside the nanocrystals [8]. Our result can be understood as a surface effect. Most of the Mn^{2+} ions are distributed at or near the surface of the nanocrystals, and the nearest-neighbour Mn^{2+} ions' exchange interaction is considerably weaker than that between the Mn^{2+} ion pairs inside the QDs.

The consequences of our results, that the Mn^{2+} ions have not been detected inside the $Cd_{1-x}Mn_xS$ nanocrystals, are the absence of the stronger Mn–Mn exchange interaction and the absence of the Mn^{2+}-based fluorescence band. On the other hand, the Mn^{2+} ions introduced on the surface of the nanocrystals produce passivation of defect centres on the surface of CdS QDs and the disappearance of the long wavelength emission, which could be useful in some applications. This seems to be a general feature of these quantum dots systems: the addition of the Mn^{2+} ions to the outside of ZnS nanoclusters reduces significantly the blue emission originating from the ZnS defect states, and promotes the near-band gap emission [5].

4. Conclusion

A colloid chemistry based procedure was developed for the synthesis of $Cd_{1-x}Mn_xS$ QDs with diameter $d \leqslant 4.5$ nm. The onset of optical absorption in $Cd_{1-x}Mn_xS$ QDs is shifted to higher energies compared to the bulk crystal with the same manganese content. The band gap

energy obtained from the room temperature absorption spectra does not vary monotonically with increasing manganese concentration. The presence of Mn^{2+} ions in CdS QDs induces the disappearance of the emission band in the room temperature fluorescence spectrum, which is attributed to the defect centres on the surface of CdS QDs. The EPR spectra show that most of the Mn^{2+} ions are distributed at or near the surface of the nanocrystals. Isolated Mn^{2+} ions with enhanced hyperfine splitting are detected for all the manganese concentrations, and the maximum number of isolated ions is observed for composition $x = 0.10$. The wide line originates from the unresolved manganese transitions broadened by the crystal field on the perturbed Mn sites. The nearest-neighbour Mn^{2+} ion exchange interaction has no significant influence on the broad resonance linewidth.

Acknowledgments

Financial support for this study was granted by the Ministry of Science, Technology and Development of the Republic of Serbia, projects No 1969 and No 1996.

References

[1] Brus L E 1984 *J. Chem. Phys.* **80** 4403
[2] Rosseti R, Ellison J L, Gibson J M and Brus L E 1984 *J. Chem. Phys.* **80** 4464
[3] Wang Y and Herron N 1991 *J. Phys. Chem.* **95** 525
[4] Murray C B, Norris D J and Bawendi M G 1993 *J. Am. Chem. Soc.* **115** 8706
[5] Sooklal K, Cullum B S, Angel S M and Myrphy C J 1996 *J. Phys. Chem.* **100** 4551
[6] Bhargava R N, Gallagher D, Hong X and Nurmikko A 1994 *Phys. Rev. Lett.* **72** 416
[7] Norris D J, Yao N, Charcnock F T and Kennedy T A 2001 *Nano Lett.* **1** 3
[8] Feltin N, Levy L, Ingert D and Pileni M P 1999 *J. Phys. Chem.* B **103** 4
[9] Levy L, Feltin N, Ingert D and Pileni M P 1997 *J. Phys. Chem.* B **101** 9153
[10] Mikulec F V, Kuno M, Bennati M, Hall D A, Griffin R G and Bawendi M G 2000 *J. Am. Chem. Soc.* **122** 2532
[11] Banarjee R, Jayakrishnan R and Ayyub P 2000 *J. Phys.: Condens. Matter* **12** 10647
[12] Ikeda M, Itoh K and Sato H 1968 *J. Phys. Soc. Japan* **25** 455
[13] Bylsma R B, Becker W M, Kossut J, Debska U and Yoder-Short D 1986 *Phys. Rev.* B **33** 8207
[14] Motte L, Petit C, Boulanger L, Lixon P and Pileni M P 1992 *Langmuir* **8** 1049
[15] Pileni M P, Motte L and Petit C 1992 *Chem. Mater.* **4** 338
[16] de Wijn H W and van Balderen R F 1967 *J. Chem. Phys.* **46** 1381
[17] Igarashi T, Isobe T and Senna M 1997 *Phys. Rev.* B **56** 6444
[18] Counio G, Esnouf S, Gacoin T and Boilot J P 1996 *J. Phys. Chem.* **100** 20021
[19] Kennedy T A, Glaser E R, Klein P B and Bhargava R N 1995 *Phys. Rev.* B **52** R14356
[20] Dorain P B 1958 *Phys. Rev.* **112** 1058